

Rethinking Uncertainty Quantification and Entanglement in Image Segmentation

Jakob Lønborg Christensen¹[0009-0001-1510-6081], Vedrana Andersen Dahl¹[0000-0001-6734-5570], Morten Rieger Hannemose¹[0000-0002-9956-9226], Anders Bjorholm Dahl¹[0000-0002-0068-8170], and Christian F. Baumgartner²[0000-0002-3629-4384]

¹ Technical University of Denmark, DTU Compute

² University of Lucerne, Faculty of Health Sciences and Medicine, Switzerland

Abstract. Uncertainty quantification (UQ) is crucial in safety-critical applications such as medical image segmentation. Total uncertainty is typically decomposed into data-related aleatoric uncertainty (AU) and model-related epistemic uncertainty (EU). Many methods exist for modeling AU (such as Probabilistic UNet, Diffusion) and EU (such as ensembles, MC Dropout), but it is unclear how they interact when combined. Additionally, recent work has revealed substantial entanglement between AU and EU, undermining the interpretability and practical usefulness of the decomposition. We present a comprehensive empirical study covering a broad range of AU-EU model combinations, propose a metric to quantify uncertainty entanglement, and evaluate both across downstream UQ tasks. For out-of-distribution detection, ensembles exhibit consistently lower entanglement and superior performance. For ambiguity modeling and calibration the best models are dataset-dependent, with softmax/SSN-based methods performing well and Probabilistic UNets being less entangled. A softmax ensemble fares remarkably well on all tasks. Finally, we analyze potential sources of uncertainty entanglement and outline directions for mitigating this effect.

Keywords: Image Segmentation · Uncertainty Quantification · Uncertainty Entanglement · Aleatoric · Epistemic

1 Introduction

When using machine learning models in high-stakes environments such as medical imaging, knowing *that* a model is uncertain is insufficient; we must also understand *why*. Is the underlying data inherently ambiguous, or has the model simply not encountered enough similar examples? Uncertainty quantification (UQ) theory addresses this by distinguishing between aleatoric uncertainty (AU, or data-driven) and epistemic uncertainty (EU, or model-driven). Despite this theoretical framework, empirical studies consistently show that the "correct" uncertainty measure for a specific task is often outperformed by the "wrong" one [16, 17, 26]. This discrepancy arises because these two sources, which should

be independent in theory, are frequently entangled in practice. To advance safe machine learning, we need to identify the sources of this entanglement and develop strategies to fix it.

The total uncertainty of a system is given by $TU = AU + EU$. As more data are observed, epistemic uncertainty can be reduced, while aleatoric uncertainty remains irreducible [19] for a given dataset. These uncertainty measures are used for various downstream tasks, such as ambiguity modeling (AMB), out-of-distribution detection (OODD), model calibration (CAL), failure detection, and active learning [17]. We focus on AMB, OODD and CAL, as each relates to one of the three measures. In theory, AMB, OODD and CAL are best addressed by AU, EU and TU, respectively. In practice, however, the measures are often entangled [16, 17, 26] and it is not clear which measure is best for which task, with a large dependency on dataset and model choice [17]. High entanglement obscures the true source of uncertainty, potentially undermining downstream task performance and leading to safety-critical mistakes. The literature points to multiple sources of this uncertainty entanglement, such as the functional form of the uncertainties [35] or the loss minimization inherent to deep learning [4]. Additionally, large models exhibit epistemic collapse, with EU vanishing as network size increases [10, 20], making TU increasingly correlated with AU.

AU is commonly modeled with probabilistic generative models [21, 25, 28], while EU is captured by inducing distributions over model parameters [11, 23, 24]. Although these can be combined [5, 7, 36], it remains unclear whether modeling both is necessary. Some studies suggest AU alone suffices [17], while others argue EU is important for OODD performance [36]. Moreover, it is unclear which combinations of EU and AU approaches yield the best results.

To address the many unknowns in the field, we provide a comprehensive empirical study focusing on the combination of aleatoric and epistemic uncertainty quantification for image segmentation. Our main contributions are as follows:

- Building on the ValUES [17] uncertainty quantification framework, we propose an entanglement metric Δ that quantifies whether the theoretically correct uncertainty measure outperforms the wrong one for a given task.
- We perform a rigorous evaluation of 4×5 AU-EU model combinations on the Cháksu IMAGE and LIDC-IDRI datasets across 3 downstream tasks.
- We provide task-specific model recommendations, balancing entanglement and performance.
- We analyze sources of uncertainty entanglement and suggest directions for mitigation.

2 Background

Multiple approaches have been proposed to estimate aleatoric and epistemic uncertainty in deep learning [19, 30]. One influential approach is the information-theoretic framework proposed by Kendall and Gal [19], which models both types of uncertainty in a unified manner. This framework has been widely adopted

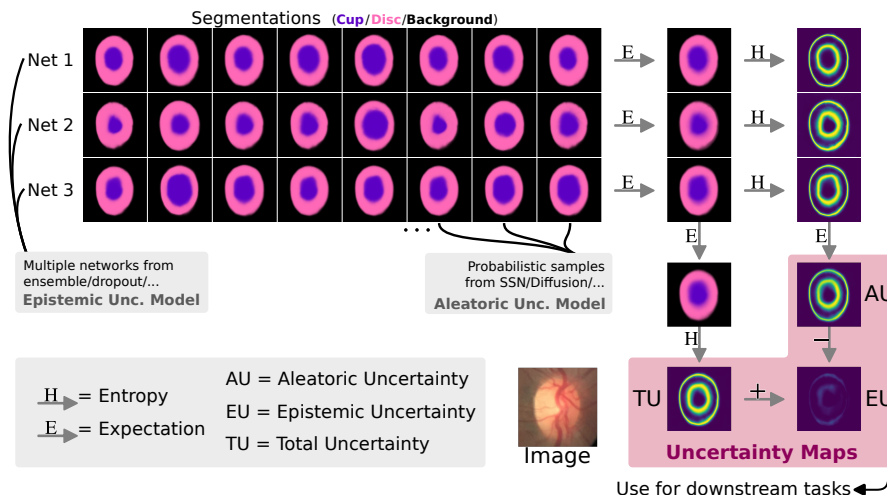


Fig. 1: A visualization of aleatoric and epistemic modeling components and their aggregation into uncertainty measures for downstream tasks.

in classification and image segmentation [16, 26, 36]. Let $p = p(y|x, \theta)$ be the predictive distribution of a model for input x and classification output y given network parameters θ . Then, the uncertainty components can be expressed as

$$AU = \underbrace{\mathbb{E}_{\theta}[H(\mathbb{E}_y[p])]}_{\text{Expected Entropy}}, \quad TU = \underbrace{H(\mathbb{E}_{\theta}[\mathbb{E}_y[p]])}_{\text{Predictive Entropy}}, \quad EU = \underbrace{TU - AU}_{\text{Mutual Information}}, \quad (1)$$

where $H = \sum_i -p_i \log p_i$ is the Shannon entropy. Here, $\mathbb{E}_y[p]$ is the Bayesian model average (BMA), i.e. the average of samples produced by a model. For deterministic models (“softmax”), the output already approximates the BMA, so the expectation over y collapses. The equations are visualized in Fig. 1.

AU models for segmentation include the Stochastic Segmentation Network (SSN) [25], Prob. UNet [21], TTA [3] and Diffusion [1, 28]. These function independently of EU methods such as deep ensembles [23], MC dropout [11] and SWA/SWAG [15, 24], allowing straightforward combination [7, 18]. For example, Zepf et al. [36] combined SSNs with Laplacian approximation of model weights, Wang et al. [34] combined TTA with dropout, and Chan et al. [5] combined diffusion with a Bayesian hyper-network. Which combinations synergize well for which tasks remains an open question.

Many works have demonstrated uncertainty entanglement [4, 16, 33, 35], with ValUES [17] being the most comprehensive empirical study for image segmentation. ValUES evaluates a wide range of uncertainty quantification methods on multiple datasets and downstream tasks, showing that the ideal uncertainty measure is often not the best performing one, with strong dataset and model dependency. While methods can model simulated toy data accurately, entanglement is prevalent on real data. ValUES also used variational model outputs (e.g.

Dataset	Modality	n_c	Ims	Ann/Im	Train	Val	Test (ID/OOD)
LIDC-IDRI	CT	2	15096	4	9355	2689	3052 / 3052×4
Chákşu IMAGE	Fundus	3	1345	5	648	162	264 / 271

Table 1: Summary of the datasets used in our experiments (n_c :=number of classes).

SSN) directly as the BMA, arguing that AU and EU labels should be swapped since sample variability captures AU rather than EU. A major limitation of ValUES is that it neglects the interplay between AU and EU by using either aleatoric (SSN/TTA) or epistemic (dropout/ensemble) approaches separately rather than in combination. Furthermore, ValUES simulated aleatoric uncertainty via random label flipping on Cityscapes [9]/GTA V [29], which is a poor simulation since a simple hand-coded model head could capture this ambiguity perfectly.

3 Methods

3.1 Data

UQ methods for segmentation can be optimally evaluated using data with multiple annotations per image. Such data captures aleatoric uncertainty through annotator disagreement, and therefore allows for more principled evaluation of AMB and CAL [21]. In our benchmark, we use the following two multi-annotator datasets: the LIDC-IDRI CT lung nodule dataset and the Chákşu IMAGE fundus photography glaucoma dataset. While LIDC-IDRI is originally a 3D dataset we use a version based on 2D slices for better comparability with Chákşu IMAGE.

The LIDC-IDRI dataset [2] (**LIDC**) consists of 1018 thoracic CT scans with annotated lung nodules (see Fig. 2). Each scan is annotated by at least four radiologists. For 2D segmentation, 15,096 slices with exactly 4 annotations are commonly used [8,21,25,28]. Slices are cropped to 128×128 pixels centered on the lesion and split per-patient into 60%/20%/20% train/val/test sets. Notably, annotator disagreement in LIDC is dominated by nodule presence/absence rather than boundary delineation. We apply four synthetic OOD shifts (blur, noise, contrast, JPEG compression) to all test images of the LIDC data, yielding one ID and four OOD test sets.

The Chákşu IMAGE dataset [22] (**Chaksu**) consists of 1345 RGB fundus images with annotated optic disc and optic cup segmentations (see Fig. 3). Each image is annotated by 5 ophthalmologists. To filter annotation errors, we only keep the largest connected component of each annotation. The data was captured using three devices: Remidio, Bosch and Forus with 1074, 145 and 126 images, respectively. The Remidio data serves as ID and Bosch/Forus as OOD. We use the original test split (264 ID test images) and split the remaining 810 ID images 80/20 into training and validation. The images are cropped around the optic disc and cup region, with per-device normalized crop sizes to ensure the OOD-shift

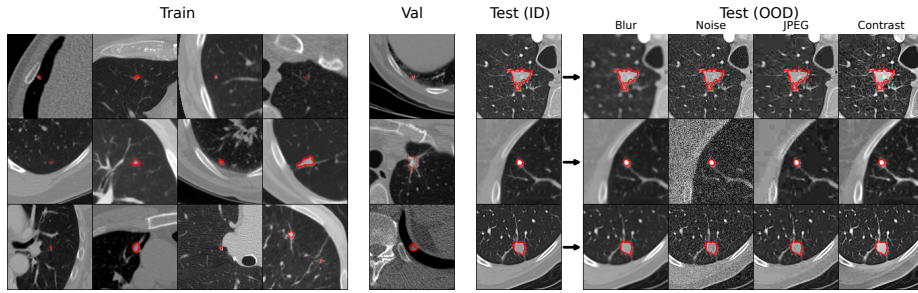


Fig. 2: Example images from the LIDC-IDRI dataset, showing the 4 annotator delineations for lung nodules as red lines.

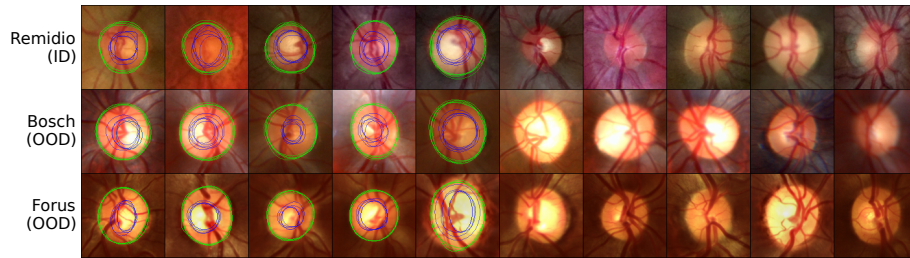


Fig. 3: Example images from the Chaksu dataset, showing the 5 annotator delineations for cup and disc as blue and green lines respectively (for the first 5 images). Each row is data from a different scanning device.

reflects image characteristics rather than size differences. The crop side length is set to twice the device average bounding box sidelength. All images are resized to 128×128 pixels.

3.2 Aleatoric and Epistemic Uncertainty Models

Here, we describe all models and hyper-parameter settings used in our experiments. We investigated the following methods for AU estimation:

- **Softmax:** A deterministic UNet trained with a standard cross-entropy loss. Referred to as "softmax" for the softmax output layer giving rise to the probabilities used in the uncertainty measures.
- **Stochastic Segmentation Networks (SSN)** [25]: A stochastic segmentation network, modeling the logits as a Gaussian distribution with a mean and variance output by the network. We use a rank of 10 for the covariance matrix, $\epsilon = 1e-5$ for numerical stability and 10 pretraining epochs estimating the mean before also modeling the variance.
- **Probabilistic UNet (Prob. UNet)** [21]: A probabilistic UNet with prior and posterior encoder networks, trained with KL divergence as an additional

loss term. We use a latent dimension of 6, $\beta = 5e-4$ (LIDC) and $\beta = 2.5e-3$ (Chaksu) for the KL weight, with linear warmup over the first 32 epochs. Our β values are smaller than typical because we use mean rather than sum reduction for the reconstruction term.

- **Diffusion** [1, 8, 12]: A diffusion model learning to reverse a noising process, trained with uniform MSE loss weights in the data domain with a softmax head. The cosine noise schedule is used with input scaling [6] at $b = 0.1$. For inference, we use the DDIM [31] sampler with 10 timesteps.

For the EU estimation we studied the following approaches:

- **Deep Ensemble (Ensemble)** [23]: A deep ensemble of 5 models, each trained from different random initializations.
- **MC Dropout (Dropout)** [11]: A single model with channel-wise [32] dropout (rate 0.2) applied before convolutional layers in residual blocks, activated at both train and test time.
- **Stochastic Weight Averaging-Gaussian (SWAG)** [24]: SWAG approximates the weight posterior by fitting a Gaussian to weights collected during training. We use 30 snapshots from the last 30 epochs with AdamW instead of SGD, which performed better in early testing. The diagonal-only variant is referred to as **SWAG-D**.
- **No EU**: No epistemic modeling; the AU model’s generative outputs are used directly following ValUES [17], without swapping AU and EU labels.

All model combinations are valid except softmax without EU, which produces only deterministic predictions incompatible with the Kendall & Gal framework [19]. For each model, we adopt hyperparameters as specified in the original literature whenever possible. When hyperparameter values are ambiguous or may depend on the dataset or network architecture, we perform limited small-scale sweeps to select appropriate settings.

3.3 Model Architecture

To reduce architecture-based variation all models share a common attention UNet architecture based on Simple Diffusion [13, 14]. The probabilistic models require modifications to the base architecture. SSN adds lightweight heads for the diagonal variance and low-rank covariances of the Gaussian logit distribution. Diffusion models add a timestep embedding passed to all residual blocks, yielding a small increase in parameters. For Prob. UNet, two extra UNet encoders serve as the prior and posterior networks. To account for the added parameters, we scale the base channels for all three Prob. UNet networks from 32 to 24. The final model sizes are 15.78, 15.80, 15.81 and 16.89 million parameters for Softmax, SSN, Diffusion and Prob. UNet, respectively.

We train all models from scratch, as using pretrained weights would be difficult for the more involved AU models (Diffusion, Prob. UNet), complicating fair comparison. Models with No EU or SWAG/SWAG-D can share a single training run since they do not affect training directly.

3.4 Uncertainty Quantification

We generally follow the ValUES [17] framework, basing experiments on the AMB, OOD detection and CAL tasks. At test time, we draw 10 AU samples and use 10 EU model instances, yielding up to 100 joint predictions per image for computing uncertainty maps via Eq. (1).

Out-of-distribution detection (OODD). OODD distinguishes ID from OOD samples using uncertainty maps, and is measured by the area under the receiver operating characteristic curve (AUROC). An aggregation strategy is needed to reduce pixel-wise maps to image-level scores. ValUES suggested three strategies: the image-wise mean, the patch-level maximum uncertainty for a 10×10 patch, and a threshold-based strategy. Larger segmentations tend to have higher uncertainty under e.g. image-wise mean, and this can lead the model into predicting that all large lung nodules in LIDC are OOD and all small nodules are ID, which is undesirable. Therefore, we add the area-normalized and border-normalized strategies. The border length is the count of 1-connectivity neighboring pixel pairs with differing labels. If area or border is zero, we normalize by 1.

Ambiguity modeling (AMB). AMB aims to capture data-inherent variance. To measure how well this variance is captured, we compute pixel-wise variance over multiple ground truth annotations and compare to predicted uncertainty maps using normalized cross-correlation (NCC), averaged across the dataset. NCC is computed separately for ID and OOD data.

Calibration (CAL). The goal of calibration is to ensure that the predicted probabilities reflect the true likelihood of correctness. We use average calibration error (ACE), which is the average absolute difference between confidence and accuracy across 20 equal-width bins from 0 to 1. The average is weighed equally across the bins, as opposed to the pixel-weighted ECE which is dominated by large low-uncertainty regions. Uncertainty measures are converted to confidences by Platt scaling [27] their negatives, with separate parameters for AU, EU and TU. Unlike ValUES, which computed Platt parameters by averaging per-image Platt parameters, we compute dataset-wide parameters. For LIDC, we also compute dataset-wide ACE instead of averaging per-image ACE, since many images have very small foreground regions leading to trivially low ACE when predicted as empty.

Entanglement (Δ). Entanglement can be identified through the relative performance of UQ measures. Specifically, if a theoretically non-appropriate measure outperforms the theoretically appropriate one for a given task, it indicates an underlying coupling between them. To quantify this behavior, we define our entanglement measure as:

$$\Delta = s \frac{\arctan(U_c/U_w) - \pi/4}{\pi/4} = s \frac{\phi}{\pi/4}, \quad (2)$$

where U_c and U_w are the performance of the correct and wrong uncertainty measures, respectively. For metrics where a lower value is better, such as ACE,

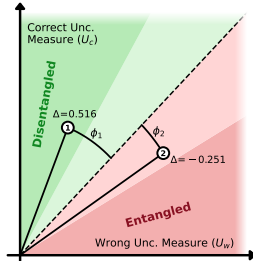


Fig. 4: A visualization of the entanglement measure Δ , shown for an uncertainty measure where higher is better. Point 1 is disentangled, while point 2 is entangled. The metric is proportional to the signed angles (shown as ϕ_1 and ϕ_2) to the $U_c = U_w$ line.

we set $s = -1$ and otherwise $s = 1$. The metric ranges from -1 to 1 with larger values indicating better disentanglement (see Fig. 4).

3.5 Training Details

All models were trained with the AdamW optimizer, a learning rate of $1e-4$, no weight decay, a batch size of 32 and gradient clipping with a maximum norm of 0.5. On LIDC, the models were trained for 1000 epochs, except Prob. UNet models which were only trained for 500 epochs due to faster overfitting. All models trained on Chaksu were trained for 500 epochs. Exponential moving average (EMA) checkpoints with a decay rate of 0.999 were used for evaluation.

4 Results

Experimental setup. We trained all 19 valid AU-EU model combinations on LIDC and Chaksu data. Predictions from the models (Fig. 5) are combined into uncertainty maps (Fig. 6) which we evaluate on the downstream tasks (OODD, AMB, CAL). CAL and AMB were evaluated on both ID and OOD data splits. OODD experiments use border-normalization as an aggregation strategy. Experiments were repeated 5 times with different seeds for Chaksu to estimate confidence intervals.

Performance and entanglement. Our central results on performance and entanglement can be seen in Fig. 7 as scatter plots in the coordinate system of the entanglement measure (Δ). The y-axis shows the theoretically correct uncertainty measure (U_c), while the x-axis shows the theoretically wrong uncertainty measure (U_w). Points below (OODD, AMB) or above (CAL) the $x = y$ line thus represent model combinations for which wrong uncertainty is better for a given task. We find that, as theoretically predicted, U_c is better than U_w for majority of models and tasks. Ensembles perform remarkably well, both in task performance and entanglement. Models with no EU component are located far from

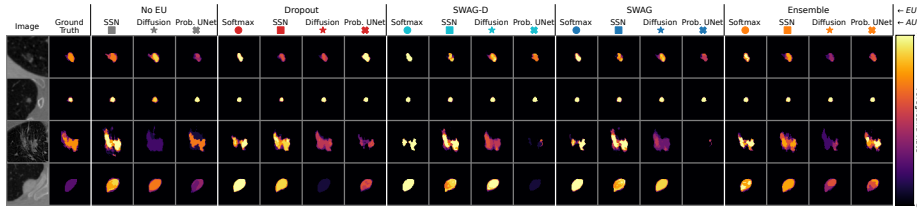


Fig. 5: Mean model predictions ($\mathbb{E}_\theta[\mathbb{E}_y[p]]$) on LIDC data (ID).

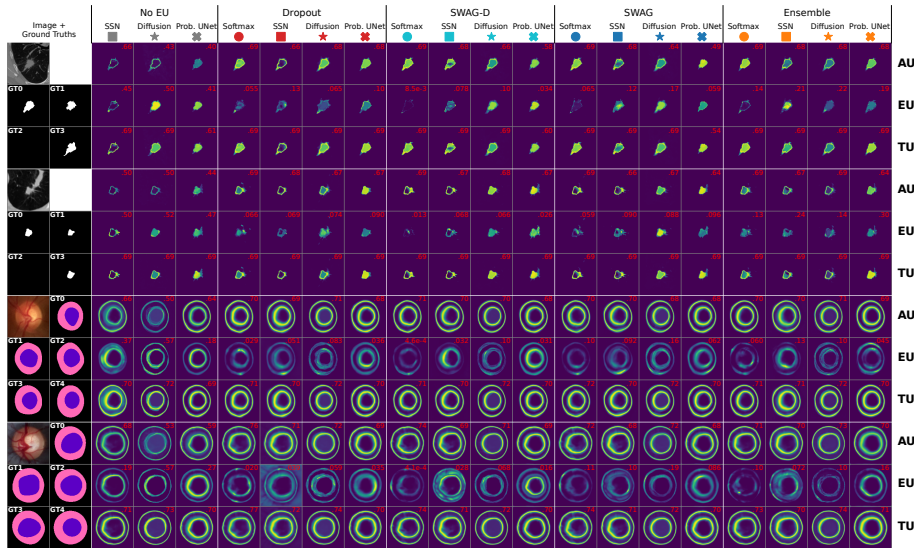
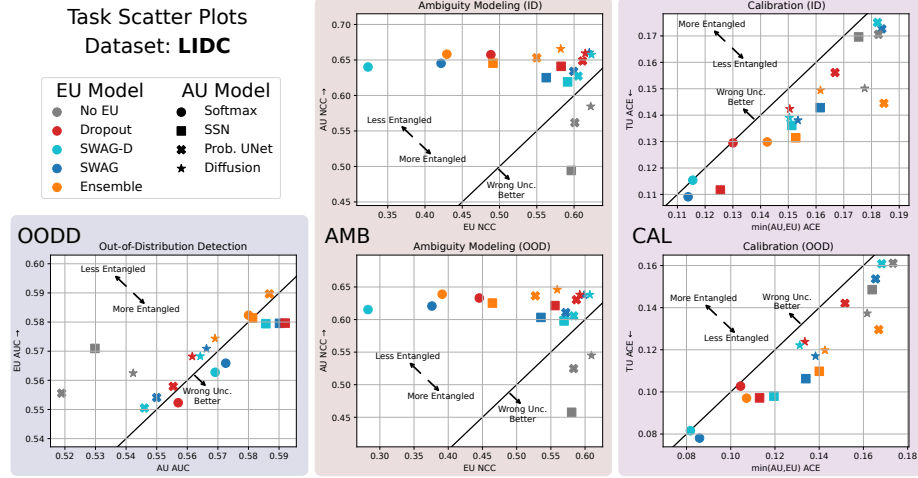


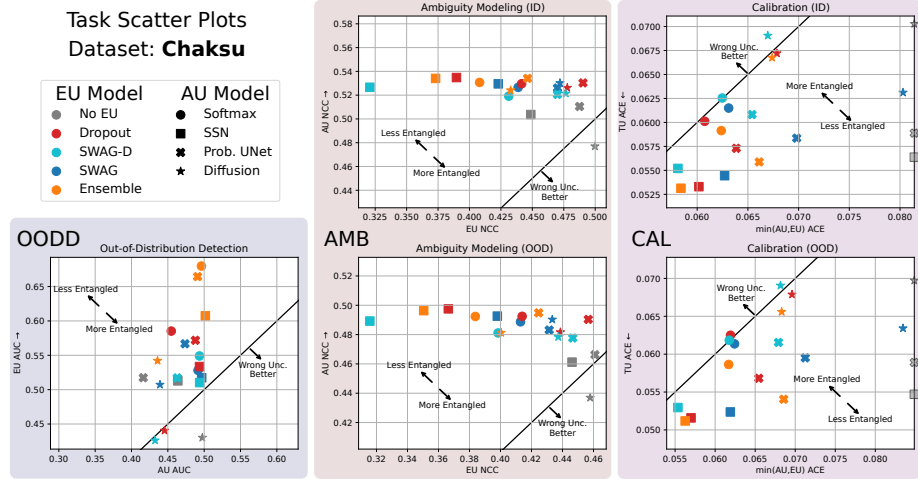
Fig. 6: Aleatoric (AU), epistemic (EU) and total uncertainty (TU) maps shown for images shown for ID images, with red numbers indicating maximum value.

other models, usually with lower performance. Softmax and SSN models do well on both AMB and CAL performance while keeping low entanglement.

AU-EU combination effects. Under the assumption that there is no entanglement between the EU and AU estimations, the OOD performance would be entirely determined by the EU model, the AMB performance would be entirely determined by the AU model, and the CAL performance would depend on both. Fig. 7 thus reveals entanglement since performance is often determined by both AU and EU model type. For OOD, ensembles cluster far from non-ensemble models. However, contrary to the theory, the non-ensemble models still show an AU dependence by forming clusters (especially on LIDC data, see Fig. 7a). In AMB, AU model type affects entanglement rather than performance: SSN and softmax are less entangled than Prob. UNet and Diffusion. Performance and entanglement in CAL is largely determined by the AU model type.



(a) Scatter plots for LIDC dataset. Metrics are calculated separately for each OOD augmentation and mean aggregated afterwards.



(b) Scatter plots for the Chaksu dataset. Softmax models in CAL were clipped (shown faded on the axis) to improve visibility of other models.

Fig. 7: Scatter plots showing the performance of model combinations on the different tasks (OODD, AMB, CAL). The AMB and CAL tasks are shown for both ID and OOD data splits. Each point corresponds to a model combination, with y-values based on the ideal uncertainty measure and x-values using the “wrong” uncertainty.

Perf. Rank		AU Method							
		Soft-max	SSN	Prob. UNet		Diff.	Soft-max	SSN	Prob. UNet
EU Method	No EU	N/A	14.3	17.3	15.0	N/A	12.3±0.8	12.6±1.6	18.5±0.7
	Dropout	9.8	5.8	12.7	8.3	7.4±1.5	5.2±1.2	6.5±2.1	15.3±1.3
	SWAG-D	9.2	9.3	17.2	8.2	11.1±0.6	8.2±1.2	11.9±2.0	16.7±0.6
	SWAG	7.8	9.7	15.8	7.0	9.9±1.1	7.6±0.5	8.6±2.5	11.5±2.8
	Ensemble	3.0	6.3	6.7	6.5	5.0±0.9	3.5±0.7	3.5±0.9	14.7±0.7

LIDC

Chaksu

(a) Ranking of the model performance (EU AUC, AU NCC, TU ACE).

Ent. (Δ) Rank		AU Method							
		Soft-max	SSN	Prob. UNet		Diff.	Soft-max	SSN	Prob. UNet
EU Method	No EU	N/A	11.2	10.7	8.3	N/A	8.6±1.2	7.7±1.9	13.6±0.3
	Dropout	12.0	11.5	12.2	9.0	9.3±0.5	8.9±1.7	10.3±1.3	14.7±1.7
	SWAG-D	12.0	11.8	12.8	11.7	11.4±2.6	9.4±1.1	12.2±2.7	16.0±1.3
	SWAG	10.8	9.8	11.2	8.3	11.7±2.4	9.3±1.6	9.0±1.3	9.1±1.9
	Ensemble	7.7	6.8	5.7	6.5	5.9±1.0	6.8±1.5	5.9±0.8	10.5±2.1

LIDC

Chaksu

(b) Ranking of the entanglement metric (Δ).

Table 2: Average ranking (1-19) of performance and entanglement (Δ) when comparing the 19 AU-EU model combinations. The ranks were calculated separately per task and data split, then averaged across ID/OOD splits, and finally averaged across tasks. Numbers after \pm are student T-test uncertainty intervals for the mean ($N = 5$ seeds).

Ranking overview. We rank all models by their correct-metric performance (EU AUC, AU NCC, TU ACE) and by Δ , averaging ranks across tasks. Results (Tab. 2) confirm ensembles rank best overall, with dropout slightly outperforming SWAG/SWAG-D among cheaper alternatives. On Chaksu, SSN/Prob. UNet ensembles perform well, while softmax ensembles perform best on LIDC. If reducing entanglement is a priority, ensembles seems to be the best choice, but the AU-method is a tossup between softmax, SSN and Prob. UNet.

Epistemic collapse. Epistemic collapse causes EU component models to mostly predict the same BMA. As a result, the magnitude of EU maps are far smaller than AU maps, meaning $TU \approx AU$ which causes problems for CAL. With the exception of the "no EU" models, the EU/AU ratio is always less than 1 (see Fig. 8). The problem is more severe for dropout and SWAG-D than SWAG and ensembles. Softmax models are significantly more affected by epistemic collapse.

OODD Aggregation strategy. We ablate the aggregation strategy for OODD (Fig. 9), finding it matters only for LIDC and not Chaksu. Chaksu models cluster similarly across strategies, likely because the dataset is more

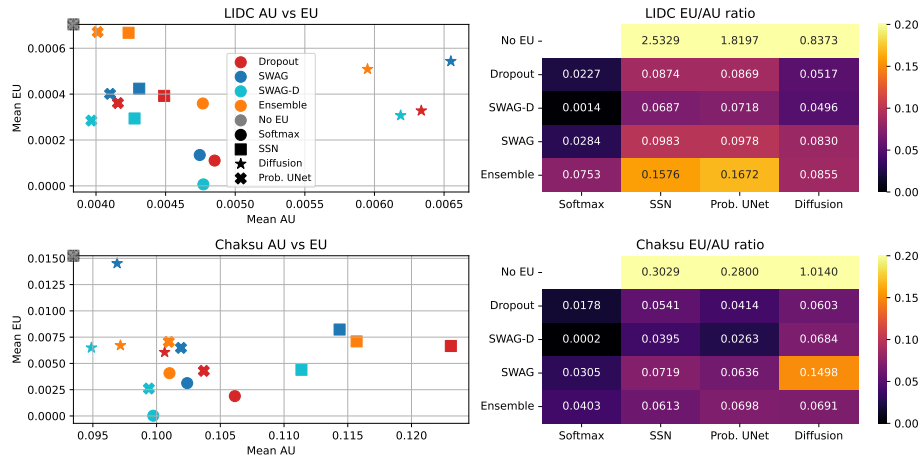


Fig. 8: Left: Scatter plots comparing mean AU and EU across models and datasets. Right: Mean ratio of EU/AU across models and datasets (OOD split). Standard image-wise mean was used to reduce uncertainty images to single numbers.

class-balanced with no empty labels. For LIDC, border-normalization outperforms alternatives while threshold-based normalization performs worst. Methods that better account for mask size variation perform better. Notably, better-performing aggregation methods also exhibit higher entanglement, improving AU AUC faster than EU AUC.

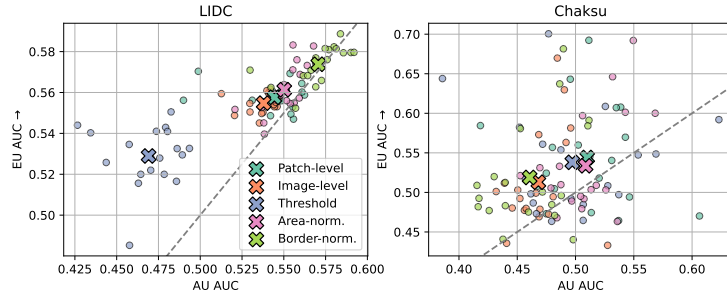


Fig. 9: Scatter plots showing OOD performance as different aggregation strategies are used. Each small point is an AU-EU model combination, and the large crosses are the mean performances across all combinations.

	Performance	Entanglement (Δ)	Both
Out-of-distribution detection (OODD)	Prob. UNet ens. /Softmax ens.	Prob. UNet ens. /Softmax ens.	Prob. UNet ens. /Softmax ens.
Ambiguity Modeling (AMB)	Softmax ens.	Softmax ens.	Softmax ens.
Calibration (CAL)	SSN dropout	Prob. UNet ens.	SSN dropout /SSN ens.
Overall	Softmax ens.	Prob. UNet ens.	Prob. UNet ens. /Softmax ens.

Table 3: Our recommendations for AU-EU model combinations across tasks, based on whether performance, low entanglement or both are important. AU-EU model combinations are assigned colors for an easy overview.

5 Discussion

Epistemic collapse as a source of entanglement. EU magnitudes are substantially smaller than AU for nearly all models (epistemic collapse). Since TU is largely fixed (entropy of the mean prediction), EU collapsing toward zero forces AU to absorb uncertainty to balance $TU = AU + EU$, directly causing entanglement. This is especially problematic for CAL, where $TU \approx AU$ prevents TU from providing information beyond AU. Addressing epistemic collapse could directly reduce entanglement. Kirsch et al. [20] proposed extracting independent sub-networks post-training, and incorporating their methods in our framework is a promising way forward. Alternatively, a simple post-hoc correction could boost EU (*e.g.* by multiplying with the mean AU/EU ratio) before computing TU, thereby making the two components more comparable in magnitude.

Low entanglement in ensembles. Ensembles exhibit the best performance and lowest entanglement across most tasks. A plausible explanation is that each ensemble member follows an independent training trajectory from a different random initialization, leading to genuinely diverse network weights and predictions. Dropout and SWAG/SWAG-D obtain weight distributions from a single training run, constraining model diversity and potentially causing EU to capture less epistemic variation, which leaks into AU, causing entanglement. We observe less severe epistemic collapse for ensembles, supporting this hypothesis.

Models without an EU component. No EU models are consistently outliers in Fig. 7: more entangled in OODD and CAL, less entangled in AMB, with generally worse performance. Since their generative predictions serve directly as the BMA, epistemic collapse does not apply, explaining their lower CAL entanglement. Otherwise, these models show no clear trends consistent with a meaningful AU-EU decomposition. We therefore argue against applying the Kendall & Gal decomposition to models without an explicit EU component, as done in ValUES [17]. To our knowledge, this application lacks a formal theoretical foundation in existing literature, and we therefore caution against it.

Model choice recommendations. Model selection involves trading off performance, entanglement and computational cost. Ensembles ($N = 5$ models) are the most expensive; dropout and SWAG/SWAG-D require a single training run, with SWAG needing more storage. Among non-ensemble EU methods, dropout performs slightly better overall. For OODD, ensembles excel, with the best performance and lowest entanglement. For AMB, softmax and SSN are less entangled with similar performance across EU methods. For CAL, softmax and SSN perform best while Prob. UNet is least entangled. The EU choice for AMB and CAL is data-dependent. Overall, a softmax ensemble performs surprisingly well, considering its conceptual simplicity. Without considering compute budget and easy-of-implementation, we outline our model recommendations in Tab. 3.

Limitations and future directions. Our study has several limitations. Tracking how entanglement evolves during training could shed light on when and why it emerges. Studying entanglement as a function of model size would clarify the role of epistemic collapse, which worsens with increasing capacity [10, 20]. Incorporating non-generative AU methods such as TTA [3] would test whether trends generalize beyond probabilistic models. Further, our evaluation is limited to two medical imaging datasets, each with their own flaws. The aleatoric uncertainty in LIDC is not ideal since nodules are either present or not, with little room for ambiguous mask delineations to have an effect. The OOD-shift for LIDC was simulated with augmentations, and while synthetic in nature, we preferred it to the approach by ValUES. Their feature based OOD-splits (texture, malignancy) dramatically reduced dataset size, and we found the OOD images to be inherently ambiguous, thus complicating entanglement further by having OOD images with more aleatoric uncertainty. Chaksu is relatively small with just 1345 images. Both the LIDC and Chaksu data is cropped centrally around the region of interest, which makes the segmentation task unnaturally easy compared to some applications. We found it challenging to find high-quality large scale datasets that include multiple expert annotations, which are necessary under the ValUES framework. Future work should focus some of their efforts on acquiring high quality datasets with multiple annotators, to validate the generality of our findings.

6 Conclusion

Our systematic evaluation of 19 AU-EU model combinations has shed light on the usefulness of these approaches and the challenges in uncertainty quantification. Our proposed entanglement measure quantifies whether the correct uncertainty measure outperforms the wrong one. Deep ensembles consistently achieve the best performance and lowest entanglement. We identified epistemic collapse as a key driver of entanglement, and suggested potential mitigation strategies. Our results show that applying the Kendall & Gal decomposition to models without an explicit EU component is not well-motivated. Finally, we found that segmentation metrics such as GED do not reliably predict UQ performance, cautioning against their use as proxies for uncertainty quality. Unless a generative model is

required, our findings suggest that an ensemble of standard cross-entropy trained softmax models is sufficient for downstream task performance. Our benchmark and entanglement metric provide the tools to diagnose and reduce entanglement in future methods and ultimately develop better uncertainty quantification methods.

Acknowledgements

This work was supported by Danish Data Science Academy, which is funded by the Novo Nordisk Foundation (NNF21SA0069429) and VILLUM FONDEN (40516).

References

1. Amit, T., Nachmani, E., Shaharbany, T., Wolf, L.: Segdiff: Image segmentation with diffusion probabilistic models. arXiv preprint arXiv:2112.00390 (2021)
2. Armato, S.G.I., McLennan, G., Bidaut, L., McNitt-Gray, M.F., Meyer, C.R., Reeves, A.P., Zhao, B., Aberle, D.R., Henschke, C.I., Hoffman, E.A., Kazerooni, E.A., MacMahon, H., Van Beek, E.J.R., Yankelevitz, D., Biancardi, A.M., Bland, P.H., Brown, M.S., Engelmann, R.M., Laderach, G.E., Max, D., Pais, R.C., Qing, D.P., Roberts, R.Y., Smith, A.R., Starkey, A., Batra, P., Caligiuri, P., Farooqi, A., Gladish, G.W., Jude, C.M., Munden, R.F., Petkovska, I., Quint, L.E., Schwartz, L.H., Sundaram, B., Dodd, L.E., Fenimore, C., Gur, D., Petrick, N., Freymann, J., Kirby, J., Hughes, B., Van Castele, A., Gupte, S., Sallamm, M., Heath, M.D., Kuhn, M.H., Dharaiya, E., Burns, R., Fryd, D.S., Salganicoff, M., Anand, V., Shreter, U., Vastagh, S., Croft, B.Y.: The lung image database consortium (lidc) and image database resource initiative (idri): A completed reference database of lung nodules on ct scans. *Medical Physics* **38**(2), 915–931 (Feb 2011). <https://doi.org/10.1118/1.3528204>
3. Ayhan, M.S., Berens, P.: Test-time data augmentation for estimation of heteroscedastic aleatoric uncertainty in deep neural networks. In: *Medical imaging with deep learning* (2018)
4. Bengs, V., Hüllermeier, E., Waegeman, W.: Pitfalls of epistemic uncertainty quantification through loss minimisation. *NeurIPS* (2025)
5. Chan, M.A., Molina, M.J., Metzler, C.A.: Estimating epistemic and aleatoric uncertainty with a single model. *NeurIPS* (2024)
6. Chen, T.: On the importance of noise scheduling for diffusion models. arXiv preprint arXiv:2301.10972 (2023)
7. Chlap, P., Min, H., Dowling, J., Field, M., Cloak, K., Leong, T., Lee, M., Chu, J., Tan, J., Tran, P., Kron, T., Sidhom, M., Wiltshire, K., Keats, S., Kneebone, A., Haworth, A., Ebert, M.A., Vinod, S.K., Holloway, L.: Uncertainty estimation using a 3d probabilistic u-net for segmentation with small radiotherapy clinical trial datasets. *Computerized Medical Imaging and Graphics* **116**, 102403 (2024). <https://doi.org/https://doi.org/10.1016/j.compmedimag.2024.102403>, <https://www.sciencedirect.com/science/article/pii/S0895611124000806>
8. Christensen, J.L., Hannemose, M.R., Dahl, A.B., Dahl, V.A.: Diffusion based ambiguous image segmentation. In: *Image Analysis*. pp. 187–200. Springer Nature Switzerland (2025). https://doi.org/10.1007/978-3-031-95911-0_11
9. Cordts, M., Omran, M., Ramos, S., Rehfeld, T., Enzweiler, M., Benenson, R., Franke, U., Roth, S., Schiele, B.: The cityscapes dataset for semantic urban scene understanding. *CVPR* (2016)
10. Fellaji, M., Pennerath, F.: The epistemic uncertainty hole: an issue of bayesian neural networks (2024), <https://arxiv.org/abs/2407.01985>
11. Gal, Y., Ghahramani, Z.: Dropout as a bayesian approximation: Representing model uncertainty in deep learning. *ICML* (2016)
12. Ho, J., Jain, A., Abbeel, P.: Denoising diffusion probabilistic models. *NeurIPS abs/2006.11239* (2020)
13. Hoogeboom, E., Heek, J., Salimans, T.: Simple diffusion: End-to-end diffusion for high resolution images. *ICML* (2023)
14. Hoogeboom, E., Mensink, T., Heek, J., Lamerigts, K., Gao, R., Salimans, T.: Simpler diffusion (sid2): 1.5 fid on imagenet512 with pixel-space diffusion. *CVPR* (2025)

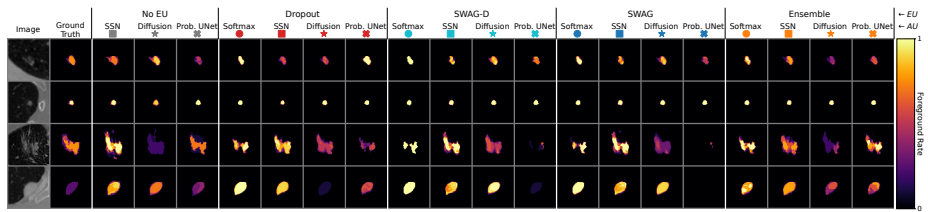
15. Izmailov, P., Podoprikin, D., Garipov, T., Vetrov, D., Wilson, A.G.: Averaging weights leads to wider optima and better generalization (2018)
16. de Jong, I.P., Sburlea, A.I., Sabatelli, M., Valdenegro-Toro, M.: Measuring uncertainty disentanglement error in classification (2025)
17. Kahl, K.C., Lüth, C.T., Zenk, M., Maier-Hein, K., Jaeger, P.F.: Values: A framework for systematic validation of uncertainty estimation in semantic segmentation. ICLR (2024)
18. Katwyk, P.V., Bergen, K.J.: Hybridflow: Quantification of aleatoric and epistemic uncertainty with a single hybrid model (2025)
19. Kendall, A., Gal, Y.: What uncertainties do we need in bayesian deep learning for computer vision? NeurIPS (2017)
20. Kirsch, A.: (implicit) ensembles of ensembles: Epistemic uncertainty collapse in large models. TMLR (2025)
21. Kohl, S.A.A., Romera-Paredes, B., Meyer, C., Fauw, J.D., Ledsam, J.R., Maier-Hein, K.H., Eslami, S.M.A., Rezende, D.J., Ronneberger, O.: A probabilistic u-net for segmentation of ambiguous images. NeurIPS (2018)
22. Kumar, J.R.H., Seelamantula, C.S., Gagan, J.H., Kamath, Y.S., Kuzhuppilly, N.I.R., Vivekanand, U., Gupta, P., Patil, S.: Chákṣu: A glaucoma specific fundus image database. Scientific Data **10**(1), 70 (2023). <https://doi.org/10.1038/s41597-023-01943-4>
23. Lakshminarayanan, B., Pritzel, A., Blundell, C.: Simple and scalable predictive uncertainty estimation using deep ensembles. NeurIPS (2017)
24. Maddox, W., Garipov, T., Izmailov, P., Vetrov, D., Wilson, A.G.: A simple baseline for bayesian uncertainty in deep learning. NeurIPS (2019)
25. Monteiro, M., Folgoc, L.L., de Castro, D.C., Pawlowski, N., Marques, B., Kamnitsas, K., van der Wilk, M., Glocker, B.: Stochastic segmentation networks: Modelling spatially correlated aleatoric uncertainty. NeurIPS (2020)
26. Mucsányi, B., Kirchhof, M., Oh, S.J.: Benchmarking uncertainty disentanglement: Specialized uncertainties for specialized tasks. NeurIPS (2024)
27. Platt, J.C.: Probabilistic outputs for support vector machines and comparisons to regularized likelihood methods. In: Advances in Large Margin Classifiers. MIT Press, Cambridge, MA, USA (1999), introduces Platt scaling as a sigmoid calibration of classifier scores
28. Rahman, A., Valanarasu, J.M.J., Hacıhaliloglu, I., Patel, V.M.: Ambiguous medical image segmentation using diffusion models. CVPR (2023)
29. Richter, S.R., Vineet, V., Roth, S., Koltun, V.: Playing for data: Ground truth from computer games. ECCV (2016)
30. Schweighofer, K., Aichberger, L., Ielanskyi, M., Hochreiter, S.: Introducing an improved information-theoretic measure of predictive uncertainty. NeurIPS (2023)
31. Song, J., Meng, C., Ermon, S.: Denoising diffusion implicit models. ICLR (2021)
32. Tompson, J., Goroshin, R., Jain, A., LeCun, Y., Bregler, C.: Efficient object localization using convolutional networks. In: CVPR (2015)
33. Valiuddin, M.M.A., van Sloun, R.J.G., Viviers, C.G.A., de With, P.H.N., van der Sommen, F.: A review of bayesian uncertainty quantification in deep probabilistic image segmentation. TMLR (2025)
34. Wang, G., Li, W., Aertsen, M., Deprest, J., Ourselin, S., Vercauteren, T.: Aleatoric uncertainty estimation with test-time augmentation for medical image segmentation with convolutional neural networks. Neurocomputing **335**, 34–45 (2019). <https://doi.org/10.1016/j.neucom.2019.01.103>, <https://pmc.ncbi.nlm.nih.gov/articles/PMC6783308/>

35. Wimmer, L., Sale, Y., Hofman, P., Bischl, B., Hüllermeier, E.: Quantifying aleatoric and epistemic uncertainty in machine learning: Are conditional entropy and mutual information appropriate measures? *UAI* (2023)
36. Zepf, K., Wanna, S., Miani, M., Moore, J., Frellsen, J., Hauberg, S., Warburg, F., Feragen, A.: Laplacian segmentation networks improve epistemic uncertainty quantification. In: *MICCAI*. Springer Nature Switzerland Cham (2024)

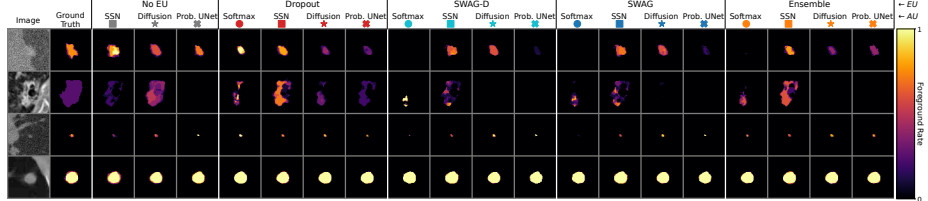
A Supplementary Materials

To supplement the paper’s findings, we have added qualitative plots showing model and dataset results, along with details on the model architecture and predictions. Due to space limits, we could not accommodate these in the main paper.

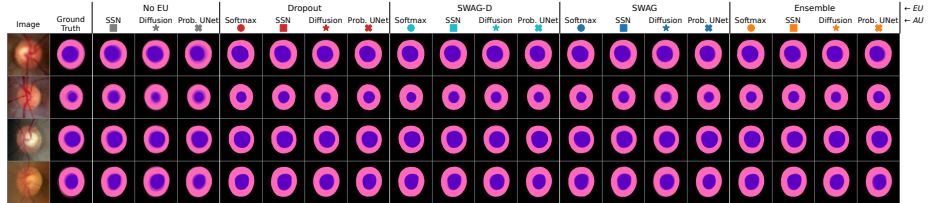
A.1 Additional Qualitative Plots



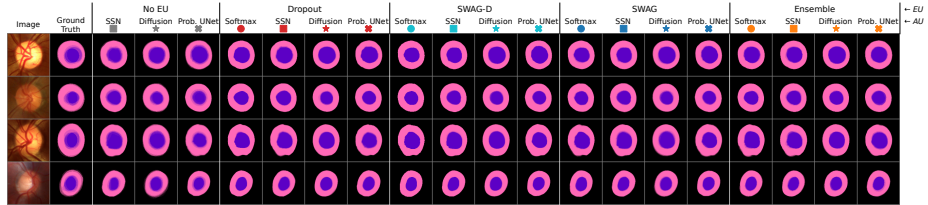
(a) LIDC dataset (ID). Repeated from the results section, but included for easier comparison.



(b) LIDC dataset (OOD).



(c) Chaksu dataset (ID). Purple, pink and black represents cup, disc and background, respectively.



(d) Chaksu dataset (OOD). Purple, pink and black represents cup, disc and background respectively.

Fig. 10: Mean predictions ($\mathbb{E}_\theta[\mathbb{E}_y[p]]$) for the different model combinations across datasets and distribution settings.

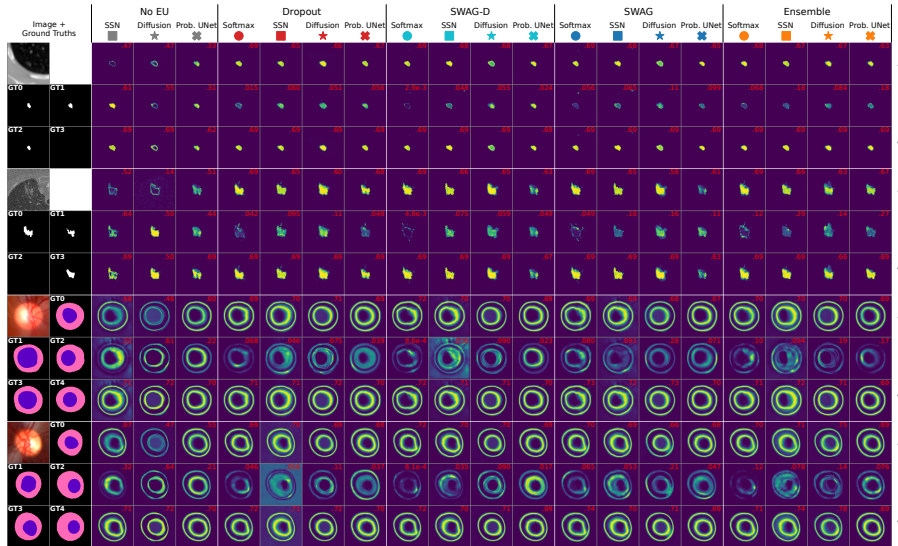


Fig. 11: Aleatoric (AU), epistemic (EU) and total uncertainty (TU) maps shown for out-of-distribution (OOD) images from the LIDC and Chaksu datasets. Red numbers indicate the maximum value. The ID variant of this plot was shown in the results section.

A.2 Architecture Details

The UNet architecture uses 32 base channels which are increased with a channel multiplier of (1, 2, 4, 8) across the different resolution scales. The backbone mainly consists of residual blocks (ResBlocks) which use the following layers:

- **Norm:** Group normalization with 32 channels and $\epsilon = 1e-5$.
- **SiLU:** The Sigmoid Linear Units, $\text{SiLU}(x) = x/(1 + e^{-x})$ (also used as activation function throughout the network)
- **Conv:** A standard 2D convolution with kernel size 3×3 .

A ResBlock is defined by sequential application of the layers: Norm, SiLU, Conv, Norm, SiLU, Conv. The ResBlocks are residual, meaning the input is added out the output. If the number of channels is changed through a ResBlock, to account of the change a 1×1 2D convolution is added to the residual path. We use 3 downscaling/upscaling operations (as implied by the channel multiplier). Downscaling uses average pooling and upscaling uses nearest-neighbour interpolation followed by a 3×3 2D convolution. Each neuron scale has 2 ResBlocks in succession, with an additional 2 middle ResBlocks. We use additive skip connections between the encoder and decoder just before/after layers with downscaling/upscaling. The number if channels is changed in the first convolution after a downscaling/upscaling operation. Self-attention is used after each ResBlock

when the neuron stack has a width of 32 or less (the two deepest scales). When applying self-attention, we consider each pixel³ as a separate token.

To enable reproducibility and specify implementation details not covered in the text, the code can be viewed at github.com/anonymous.

A.3 Discretizing Predictions

One may notice that model predictions in Fig. 1 are blurry around the edges. This reflects an intentional design choice, as we decided not to discretize model predictions. Model predictions were represented as probability maps produced by a softmax layer. Early experiments showed that converting these probability maps discrete one-hot maps with the most probable class would either hurt UQ performance or make no difference.

³ Pixel is used loosely here, referring to a spatial position in the downscaled feature tensor.

A.4 Additional Ranking Scatter Plots

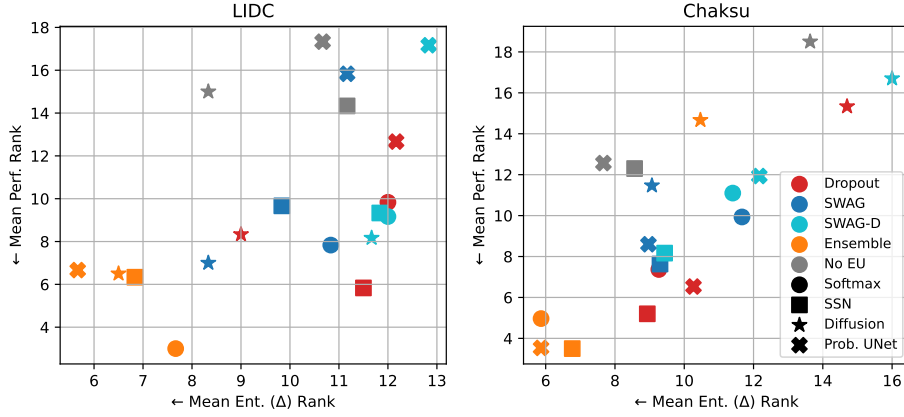


Fig. 12: A scatter plot of the mean (aggregated over tasks) performance and entanglement (Δ) ranking for different datasets.

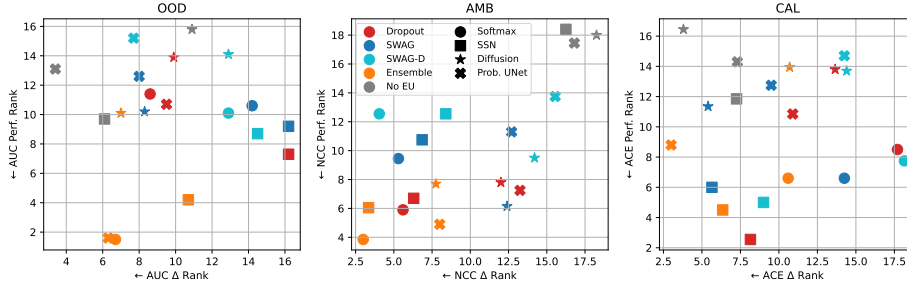


Fig. 13: A scatter plot of the mean (aggregated over datasets) performance and entanglement (Δ) ranking for different tasks.

A.5 GED and Dice Scatter Plots

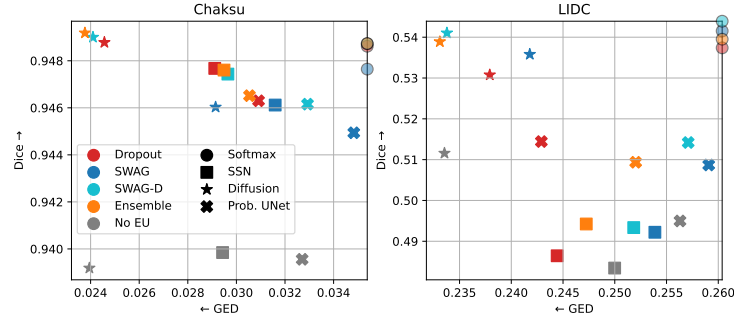


Fig. 14: A scatter plot of mean Dice vs GED scores for the different model combinations. Softmax models have been ignored for axis limits, as they are much worse in GED (indicated by faded points on the axis). Diffusion models perform strongly at these raw metrics, but the performance doesn't translate to downstream UQ tasks, as diffusion is often inferior to other AU methods.

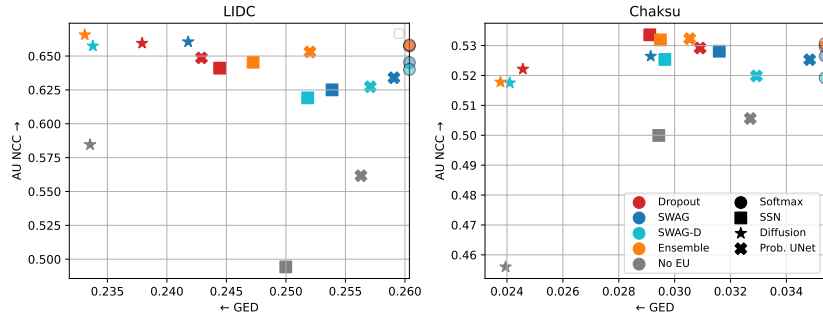


Fig. 15: A scatter plot of GED vs AU NCC for ID images. Since GED and NCC both claim to capture ambiguity modeling, we would expect a negative correlation between the measures; however, this relation is not clear. Softmax models have been ignored for axis limits, as they are much worse in GED (indicated by faded points on the axis).